NASA TECHNICAL NOTE

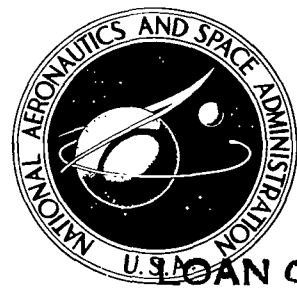

NASA TN D-7037

QUANTUM GALVANOMAGNETIC AND THERMOMAGNETIC EFFECTS IN GRAPHITE TO 18 TESLAS (180 kG) AT LOW TEMPERATURES

by John A. Woollam

Lewis Research Center
Cleveland, Ohio 44135

NATIONAL AERONAUTICS AND SPACE ADMINISTRATION • WASHINGTON, D. C. • JANUARY 1971

1. Report No. NASA TN D-7037	2. Government Accession No.	3. Recipient's Catalog No.
4. Title and Subtitle QUANTUM GALVANOMAGNETIC AND THERMOMAGNETIC EFFECTS IN GRAPHITE TO 18 TESLAS (180 kG) AT LOW TEMPERATURES		5. Report Date January 1971 6. Performing Organization Code
7. Author(s) John A. Woollam		8. Performing Organization Report No. E-5696
9. Performing Organization Name and Address Lewis Research Center National Aeronautics and Space Administration Cleveland, Ohio 44135		10. Work Unit No. 129-02 11. Contract or Grant No. 13. Type of Report and Period Covered Technical Note
12. Sponsoring Agency Name and Address National Aeronautics and Space Administration Washington, D.C. 20546		14. Sponsoring Agency Code
15. Supplementary Notes		

16. Abstract

The magnetoresistance, Hall effect, thermopower, thermal resistivity, and Nernst-Ettingshausen effects are measured in magnetic fields to 18.3 tesla (183 kG) and at temperatures between 1.1 and 4.2 K. Samples are highly ordered pressure annealed pyrolytic graphite. The major results are the assignment of majority carrier electrons and holes to specific locations in the Brillouin zone, the first observation of spin-split Landau levels, a study of distorted line shapes of thermopower quantum oscillations, and a test of Sugihara and Ono theory for Landau level crossings of the Fermi energy in graphite.

17. Key Words *(Suggested by Author(s))* Graphite; Thermomagnetic; Galvanomagnetic; Magnetothermopower; Spin-split Landau levels; Fermi surfaces	18. Distribution Statement Unclassified - unlimited

19. Security Classif. (of this report)	20. Security Classif. (of this page)	21. No. of Pages	22. Price*
Unclassified	Unclassified	34	$3.00

*For sale by the National Technical Information Service, Springfield, Virginia 22151

QUANTUM GALVANOMAGNETIC AND THERMOMAGNETIC EFFECTS IN GRAPHITE TO 18 TESLAS (180 kG) AT LOW TEMPERATURES

by John A. Woollam

Lewis Research Center

SUMMARY

The electrical magnetoresistance, Hall resistivity, adiabatic thermoelectric power, adiabatic Nernst-Ettingshausen coefficient, and thermal resistivity are measured as a function of magnetic field from 0 to 18.3 tesla (1 T = 10 kG). Temperatures range from 1.1 to 4.2 K. From the measured coefficients, the isothermal thermopower, electrical conductivity, and Hall conductivity are found. From a study of these effects, an assignment of electrons and holes to positions in the Brillouin zone is made. Spin splitting of the $n = 1$ electron Landau level is found in three of the observed coefficients. The thermopower quantum oscillations at low temperature and high magnetic field have distorted shapes. These shapes are compared with predictions of various theories, and are found to be correctly predicted by a theory by Horton. Sugihara and Ono have predicted positions in field for Landau level crossings, and we find good agreement with their predictions with the exception of the $n = 1$ electron level. A study of deHaas-van Alphen periods and anisotropy shows that majority carriers are the same as found in natural single crystals.

INTRODUCTION

Pressure annealed pyrolytic graphite is a highly ordered form of carbon (ref. 1) but is not a single crystal. The lattice for a single crystal is hexagonal. For pyrolytic samples there are individual crystallites with [0001] axes nearly parallel to each other, but [1100] axes, for example, are randomly oriented to each other. Typical crystallite size is 10- to 100-micrometer diameter. Because of the nature of the Fermi surface of graphite, the properties of pyrolytic and natural single crystals are very similar, as shown in this and other papers (ref. 2).

Fermi surface studies of natural single crystals of graphite were made by Soule,

McClure, and Smith (ref. 3) in fields to 2.4 tesla (1 T = 10 kG) using the Shubnikov-deHaas effect. deHaas - van Alphen studies on pressure annealed pyrolytic graphite were made by Williamson, Foner, and Dresselhaus (ref. 2). Magnetoreflection results (ref. 4) were used along with the deHaas - van Alphen effect to determine the magnitude of the parameters necessary to describe the energy band structure derived by Slonczewski and Weiss (SW) (ref. 5).

Soule studied the effect of boron doping on the deHaas - van Alphen frequencies (ref. 6). Boron adds positive charge and thus shifts the Fermi energy and changes the cross-sectional areas. The shifts in majority carrier frequencies assign the location of electron and hole carriers in the Brillouin zone and thus determine the signs on several of the parameters in the SW (ref. 5) band theory. Recently Schroeder, Dresselhaus, and Javan (ref. 7) have used magnetoreflection to determine the band parameter signs and find a conflict with the assignment found by majority carrier deHaas - van Alphen frequency shifts.

In this investigation two independent methods were used to determine these signs: Quantum extrema in the Hall coefficient are compared with a theory by Argyres (ref. 8) and from this a direct determination of electron and hole carrier positions in the Brillouin zone is made. This then determines the signs of the band parameters. Quantum resonances in the thermopower are used as a second and independent method of determining carrier locations and band parameter signs.

Wagoner (ref. 9) studied the electron spin resonance as a function of temperature and determined an effective g factor, which is an average over all carriers in the Brillouin zone for particular magnetic field directions. We have made the first observation of spin splitting of Landau levels in graphite. These determine the splitting at particular points in the Brillouin zone rather than an averaged value.

In this report the first studies of quantum thermomagnetic effects in graphite are made, as well as Shubnikov-deHaas studies in pyrolytic graphite. Temperatures range from 1.0 to 4.2 K and fields up to 18.3 tesla. Thermopower quantum oscillations have highly distorted line shapes and these are compared with various theories. The Shubnikov-deHaas results are compared with the theories of Adams and Holstein (ref. 10). Sugihara and Ono (ref. 11) have calculated the positions in field for Landau level crossings of the Fermi energy and show that at high fields the crossings are not predicted by strict periodicity in inverse magnetic field. Experimental and theoretical crossings are compared for each of the observed effects.

THEORY

Kinetic Equations and Transport Coefficients

The linear relations between current density $\overline{J}$, electric field $\overline{E}$, negative temperature gradient $\overline{G}$, and heat current density $\overline{w}$, may be written (ref. 12) as

$$\overline{E}^* = \hat{\rho}'\overline{J} + \hat{\epsilon}'\overline{w}^* \tag{1}$$

Adiabatic

$$\overline{G} = \hat{\pi}'\overline{J} + \hat{\gamma}\overline{w}^* \tag{2}$$

or independently as

$$\overline{E}^* = \hat{\rho}\overline{J} + \hat{\epsilon}\overline{G} \tag{3}$$

Isothermal

$$\overline{w}^* = -\hat{\pi}\overline{J} + \hat{\lambda}\overline{G} \tag{4}$$

where

$$\overline{E}^* = \overline{E} - \frac{\nabla\mu}{e} \tag{5}$$

$$\overline{w}^* = \overline{w} - \frac{\mu\overline{J}}{e} \tag{6}$$

and μ is the chemical potential. From equations (1) and (3) when $\overline{J}$ is zero

$$\hat{\epsilon}'\overline{w}^* = \hat{\epsilon}\overline{G} \tag{7}$$

where $\hat{\epsilon}$ is the isothermal thermoelectric tensor, and $\hat{\epsilon}'$ is the adiabatic thermoelectric power.

Equation (2) shows that when $\overline{J} = 0$

$$\overline{G} = \hat{\gamma}\overline{w}^* \tag{8}$$

so

$$\hat{\epsilon}' = \hat{\epsilon}\hat{\gamma} \tag{9}$$

where $\hat{\gamma}$ is the thermal-resistivity tensor and

$$\hat{\gamma} = \hat{\lambda}^{-1} \tag{10}$$

so

$$\hat{\epsilon} = \hat{\epsilon}'\hat{\lambda} \tag{11}$$

where $\hat{\lambda}$ is the thermal-conductivity tensor.

In the present experiments transport coefficients were measured as a function of magnetic field strength, temperature, and angle between the magnetic field and the C axis of graphite. The specific coefficients measured were the yy and yx components of the ρ, ϵ', and γ tensors. In addition, the following coefficients were calculated: σ_{yy} and σ_{xy} from

$$\hat{\sigma} = \hat{\rho}^{-1} \tag{12}$$

λ_{xy} and λ_{yy} from equation (10), and ϵ_{yy} from equation (11). It is important to point out that the coefficient ϵ_{yy} known as the isothermal thermopower, is the negative of the absolute thermopower or thermopower S, defined by some authors (e.g., Ziman; ref. 13). In this report, S is thermopower, not ϵ_{yy}.

Adams and Holstein Theory for σ_{yy}

Adams and Holstein (ref. 10) calculate the electrical conductivity for the case of crossed electric and magnetic fields for both degenerate and nondegenerate solids. Pertinent to this study is their calculation of the conductivity for degenerate systems in the limit of large magnetic fields and low temperatures. Their calculation is quantum mechanical in that a density matrix formalism is used.

The calculation considers various types of scattering mechanisms. At zero degrees the conductivity, valid for any particular scattering mechanism, is characterized by singularities as a function of magnetic field:

$$\sigma_{yy} \propto \sum_{n,\,m} \left(\frac{\varepsilon_F}{\hbar\omega} - n - \frac{1}{2}\right)^{-1/2} \left(\frac{\varepsilon_F}{\hbar\omega} - m - \frac{1}{2}\right)^{-1/2} \left[\begin{array}{l}\text{Terms in the square of} \\ \text{the scattering potential}\end{array}\right] \tag{13}$$

where n and m are Landau level quantum numbers and ε_F is the Fermi energy. The cyclotron frequency ω is given by

$$\omega = \frac{eH}{m^*c} \tag{14}$$

where H is magnetic field, and m* is the effective mass. The term in brackets is determined by the type of scattering. Equation (13) has infinite discontinuities where the Fermi energy and the Landau level coincide, that is, when

$$\mathcal{E}_F = \left(n + \frac{1}{2}\right)\hbar\omega \tag{15}$$

At nonzero temperatures, there is thermal and collision broadening of the Landau levels and equation (13) leads to an oscillatory part, $\tilde{\sigma}_{yy}$, of the conductivity given by

$$\tilde{\sigma}_{yy} \propto \sigma_{yy}^{o}\left(\frac{\hbar\omega}{\mathcal{E}_F}\right)^{1/2} \sum_{M} \frac{2\pi^2 MkT}{\hbar\omega}\left[\sinh\left(\frac{2\pi^2 MkT}{\hbar\omega}\right)\right]^{-1} (2\pi M)^{-1/2} \cos\left(\frac{2\pi F}{H} - \frac{\pi}{4} - \pi M\right) \tag{16}$$

where σ_{yy}^{o} is the nonoscillatory part of σ_{yy} and F is the deHaas-van Alphen frequency, proportional to the extremal cross-sectional area of the Fermi surface perpendicular to the magnetic field. The frequency F is related to $\mathcal{E}_F$ and ω by

$$\frac{F}{H} = \frac{\mathcal{E}_F}{\hbar\omega}$$

Equation (16) shows that the conductivity oscillates periodically in 1/H.

In graphite, the effective masses are so small (ref. 3) that for fields above 1 tesla terms other than the M = 1 term in equation (16) become important, and the oscillations become highly distorted. Another important feature of equation (16) is that for low temperature and high magnetic field the positions of the extrema in σ_{yy} will shift. At T = 0 K, σ_{yy} discontinuities occur at coincidence of the Fermi energy $\mathcal{E}_F$ and the Landau level. At higher temperatures the extrema move to lower fields. It is also important to know that σ_{yy} does not involve the charge of the transport carrier (ref. 9). Thus σ_{yy} is a maximum at coincidence of $\mathcal{E}_F$ and a Landau level, independent of whether carriers are electrons or holes.

Hall Conductivity Theory

Argyres (ref. 8) calculates the Hall conductivity σ_{yx} considering only elastic scattering (ionized impurity scattering, for example) in the Born approximation. The effect of both magnetic and electric fields on the collisions is considered, and, as Adams and Holstein (ref. 10) have done, he uses the density matrix formalism. For high symmetry directions of the magnetic field in graphite (parallel to the C axis, for example)

$$\sigma_{yx} = -\sigma_{xy}$$

where σ_{xy} is the Hall conductivity (ref. 12). Under these conditions Argyres results lead to

$$\sigma_{xy} \propto -q \sum_{n,k} (n+1) \left\{ \frac{f_{n+1} - f_n}{\hbar\omega} - \frac{\tau_n \left[f'_n \tau_1^{-1}(n) + f'_{n+1} \tau_1^{-1}(n+1) \right]}{\omega^2 \tau_n^2 + 1} \right\} \tag{17}$$

for isotropic scattering at $T = 0$ K. In equation (17) q is positive for holes, negative for electrons and has the magnitude of electronic charge, and

$$\tau_1^{-1} \propto \delta^{-1/2} \tag{18}$$

$$\tau_n^{-1} = \tau_1^{-1}(n) + \tau_1^{-1}(n+1) \tag{19}$$

and

$$\delta \equiv \frac{\mathcal{E}_F}{\hbar\omega} - \left(n + \frac{1}{2} \right) \tag{20}$$

In these equations f_n is the Fermi distribution function evaluated at the energy of the n^{th} Landau level and f'_n is the energy derivative of the distribution function.

Equation (17) shows that σ_{xy} has positive maxima at coincidence of $\mathcal{E}_F$ and the Landau level for electron carriers. For hole carriers σ_{xy} has negative extrema at coincidence of $\mathcal{E}_F$ and the Landau level. Thus, Hall effect quantum extrema, as a function of field, depend on charge carrier sign while conductivity extrema do not.

Horton (ref. 14) has used the density matrix approach to calculate the Hall conductivity at low temperatures and high magnetic fields. Horton's results are valid for non-zero temperatures and predict the same general result as Argyres when temperatures are low: σ_{xy} has negative extrema at coincidence of $\mathcal{E}_F$ and the Landau level for holes.

Quantum Thermopower Theory

In this section we present three approaches to the theory of quantum thermopower, in order to compare their applicability to experimental observations.

Generalized Mott equation. - The diffusion thermopower in the presence of a magnetic field is given by (ref. 15) the generalized Mott formula

$$\hat{S}(H) = \frac{\pi^2 k^2 T}{3q}\,\hat{\rho}(H)\left[\frac{\partial\sigma(H)}{\partial\mathcal{E}}\right]_{\mathcal{E}_F} \tag{21}$$

where $\hat{S}$, $\hat{\rho}$, and $\hat{\sigma}$ are field dependent tensors. As before, the factor q is positive for holes, negative for electrons, and has the magnitude of the electronic charge. By definition (refs. 12 and 13)

$$\hat{S}(H) = -\hat{\epsilon}(H) \tag{22}$$

where ϵ is defined by equation (3). Equation (21) is a result of the linearized Boltzmann equation with elastic scattering. In graphite we find experimentally

$$|\sigma_{xy}| << |\sigma_{yy}| \tag{23}$$

and

$$\left|\frac{\partial\sigma_{xy}}{\partial H}\right| << \left|\frac{\partial\sigma_{yy}}{\partial H}\right| \tag{24}$$

From symmetry,

$$\sigma_{xz} = \sigma_{yz} = \sigma_{zx} = \sigma_{zy} = 0$$

Thus,

$$S_{yy}(H) \simeq \frac{\pi^2 k^2 T}{3q}\,\frac{1}{\sigma_{yy}}\left(\frac{\partial\sigma_{yy}}{\partial\mathcal{E}}\right)_{\mathcal{E}_F} \tag{25}$$

From equations (13) and (20) combined with (25) for S_{yy}, we see that near coincidence of $\mathcal{E}_F$ with a Landau level

$$S_{yy} \propto \frac{\pi^2 k^2 T}{3q\mathcal{E}_F}\,\delta^{-1} \tag{26}$$

where δ^{-1} has positive spikes at coincidence of $\mathcal{E}_F$ and a Landau level. Thus S_{yy} will have positive spikes for hole carriers (+q) and negative spikes for electron carriers. For $T \sim 2$ K and above, the spikes in graphite become rounded maxima. Close to 4 K in graphite, S_{yy} is purely sinusoidal in 1/H.

Thermodynamic theory for S_{yy}. - To approximate the amplitude and line shape of the spike shaped oscillations that occur at low temperature and high field, we tried an

argument discussed by Callen (ref. 16), and by MacDonald (ref. 17). They find that in a steady-state condition, and where the Joule heating is small, the Thomson heat is the specific heat of the electrons per charge, as a first approximation. This assumes a reversible process or quasi-equilibrium. It then follows that the thermopower, S_{yy} is

$$S_{yy}(H) = \frac{\alpha(H)}{Nq} \tag{27}$$

where $\alpha(H)$ is the entropy of the system of electrons given by

$$\alpha(H) = -\frac{\partial\Omega(H)}{\partial T} \tag{28}$$

where $\Omega(H)$ is the free-energy of the system. Equation (27) was also derived by Obratzof (ref. 18) and others (refs. 19 and 20), but they assume that

$$|\sigma_{xy}| >> |\sigma_{yy}|$$

a condition we did not find in graphite.

Lifshitz and Kosevich (ref. 21) have evaluated Ω under conditions of strong quantization, that is, for

$$\hbar\omega >> kT$$

Using the Lifshitz-Kosevich expression for Ω, and evaluating equations (27) and (28) we find

$$S_{yy} = -\frac{2k}{qn_o}\left(\frac{eH}{ch}\right)^{3/2}\left(\frac{\partial^2 A}{\partial k_z^2}\right)_{k_z\text{-max}}^{-1/2}\sum_M \frac{e^{-MX_D}}{M^{3/2}} A_3(MX)\cos\left(\frac{2\pi MF}{H} - 2\pi M\gamma \mp \frac{\pi}{4}\right)\cos\frac{\pi Mgm^*}{2m_o} \tag{29}$$

where n_o is the density of particles, A is the extremal cross-sectional area of the Fermi surface perpendicular to the field, k_z is the component of wave vector parallel to the field, γ is a phase factor normally equal to 1/2, g is a spin factor, and X_D is the "Dingle" factor which accounts for collision broadening of Landau levels (ref. 22). The term $A_3(MX)$ is given by

$$A_3(MX) = \frac{1 - MX\coth MX}{\sinh MX} \tag{30}$$

where

$$X = \frac{2\pi^2 kT}{\hbar\omega} \tag{31}$$

The term A_3 for $M = 1$ is shown for graphite as a function of temperature at various fixed magnetic fields in figure 1, and as a function of temperature at 1 tesla for $M = 1$, 2, 3, and 4 in figure 2. From figures 1 and 2 and equation (29), it is obvious that the factor A_3 determines the amplitude and harmonic structure of the oscillations as a function of magnetic field and temperature. At low temperatures and high fields the $M = 1$ term in equation (29) decreases in relation to the $M = 2$, 3, etc., terms. This causes a highly distorted oscillation shape at low temperatures and high fields. A plot of equation (29) with parameters applicable for majority carrier holes in graphite at 2 K is shown in figure 3. Figure 3 is a plot of S_{yy} as a function of field showing distorted oscillation shapes at high fields. Equation (29) predicts better than order of magnitude agreement with experimentally observed amplitudes. However, the shape of the distorted peaks is not correctly predicted and this result will be discussed later. It is important to present the thermodynamic, Obratzof, etc. theories because the present experiments test the applicabilities of these theories to graphite.

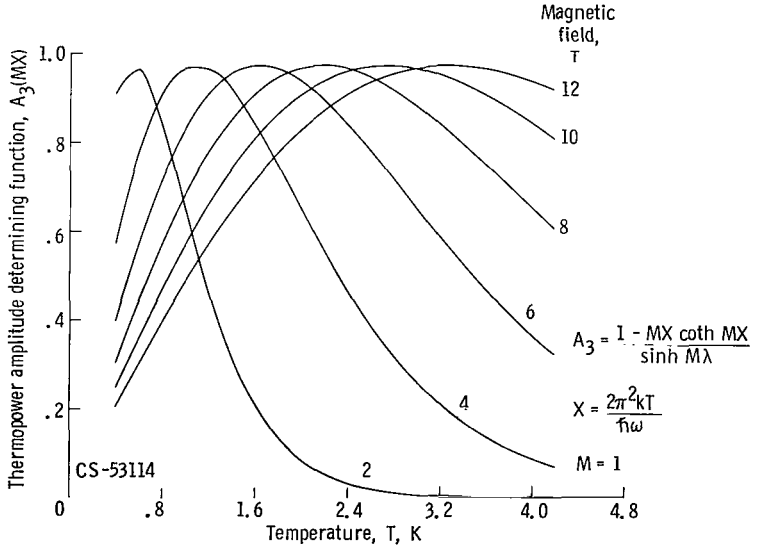

Figure 1. - $A_3(MX)$ as function of temperature (eq. (30)) for several field strengths. Effective mass, 0.04 appropriate for holes in graphite.

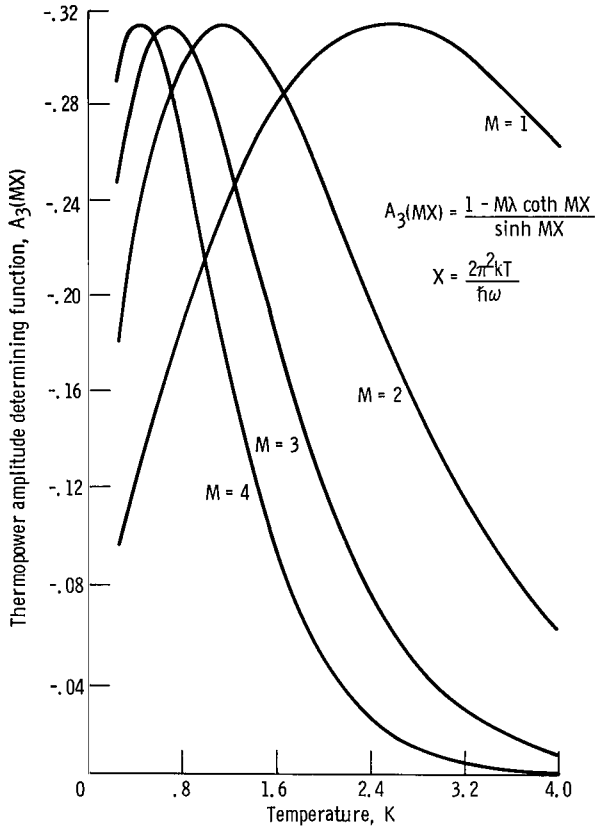

Figure 2. - $A_3(MX)$ as a function of temperature (eq. (30)) for several M values, at 1 tesla. Effective mass 0.04 m_0 appropriate for holes in graphite.

$$S_{yy} \alpha \left(\frac{eH}{ch}\right)^{3/2} \left(\frac{\partial^2 A}{\partial k_z^2}\right)^{1/2}_{k_z\text{-max}} \Sigma M \frac{e^{-MX_D}}{M^{3/2}} A_3(MX) \cos\left[\frac{2\pi MF}{H} - 2\pi M\gamma \mp \frac{\pi}{4}\right] \cos \frac{\pi M g m^*}{2m_0}$$

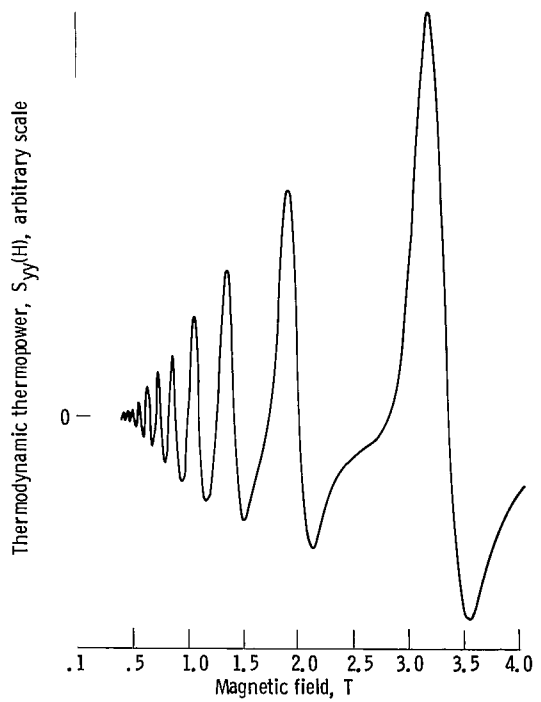

Figure 3. - Theoretical thermodynamic thermopower (eq. (29)) as function of field at 2.0 K for hole carriers in graphite.

Horton thermopower theory. - As will be discussed later, the experimentally observed distortion of oscillation peaks in thermopower is correctly predicted by a theory due to Horton (ref. 14). Horton's calculation is quantum mechanical in that he uses the density matrix formalism. Scattering is assumed to be due to random point impurities, and the calculation is for free electrons. His final expression is

$$S_{yy} = \frac{2\pi^2}{3} \frac{n_o q \tau}{m} \frac{k^2 T}{\varepsilon_F} \left[1 - \frac{15\sqrt{2}}{8\pi^2} \frac{\sqrt{\hbar\omega\varepsilon_F}}{kT} \sum_M \frac{(-1)^M}{\sqrt{M}} A_3(MX)\sin Mb \right.$$

$$\left. + \frac{45\sqrt{2}}{8\pi^2} \sqrt{\frac{\hbar\omega}{\varepsilon_F}} \sum_M \frac{(-1)^M}{\sqrt{M}} A_4(MX)\cos Mb \right] \qquad (32)$$

where

$$A_4(MX) = \frac{\pi^2}{2} \operatorname{csch}(MX)\left[2 \coth(MX) - 2MX \coth^2 MX + MX\right]$$

and A_3 is given by equation (30). The letter q is used rather than Horton's e, n_o is the charge carrier density, τ the average time between collisions, and

$$b = \frac{2\pi F}{H} - \frac{\pi}{4} \qquad (33)$$

Figure 4 shows S_{yy} from equation (32) plotted at T = 1.2 K. Figure 4 is plotted for q + (hole carriers), and there are higher positive spikes than negative dips. In part (a) a Dingle factor (eqs. (29) and (31)) was assumed with T_D = 1.0 K. In part (b) T_D = 0.5 K. As will be seen later, figure 4(b) closely approximates the experimental results. Williamson measured a T_D from deHaas - van Alphen effect of 1.5±0.1 K for a similar sample of pyrolytic graphite. This agreement supports the use of a Dingle factor in Horton's expression (introduced in eq. (29)).

Notice the highly distorted oscillation shapes in figure 4. For the same parameters the deHaas - van Alphen effect is not nearly as distorted. There are two reasons for the high distortions in thermopower. First, the A_3 term shown in figures 1 and 2 causes large harmonic content; that is, the inclusion of many of the M terms in equation (32) is necessary. The second reason is that there are two terms in equation (32). At low fields the sine term is larger, but at higher fields and low temperatures the cosine term causes significant distortion.

$$S_{yy} = 1.5\,H^{1/2} \sum_{n} \frac{(-1)^n}{n^{1/2}} A_4 \cos\left[\frac{2\pi F}{H} - \frac{\pi}{4}\right] e^{-2\pi^2 nT_D/H}$$

$$+ 79.5\,H^{1/2} \sum_{n} \frac{(-1)^n}{n^{1/2}} e^{-2\pi^2 nT_D/H} A_3 \sin\left[\frac{2\pi F}{H} - \frac{\pi}{4}\right]$$

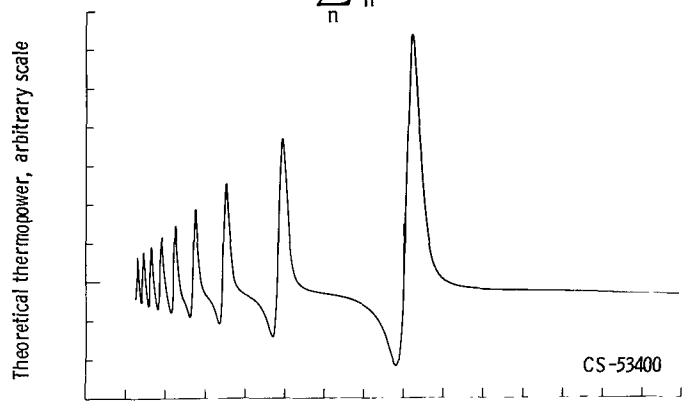

(a) Dingle temperature, 1.0 K.

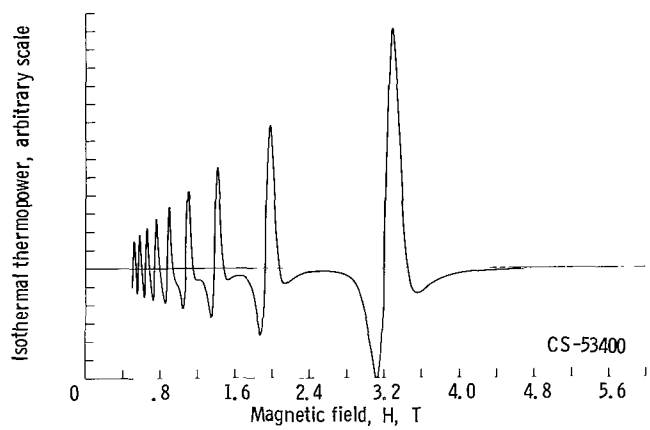

(b) Dingle temperature, 0.5 K.

Figure 4. - Theoretical Horton thermopower (eq. (32)) as function of field at 1.2 K for hole carriers in graphite.

The Energy Band Structure of Graphite

We have found, as well as others (ref. 2), that the properties of pyrolytic, pressure-annealed graphite approach the properties of natural single crystals, and in discussing the band structure will assume the two are the same.

The effective mass Hamiltonian describing the graphite energy bands was derived by Slonczewski and Weiss (SW) (ref. 5). The Hamiltonian $\mathcal{H}$ is

$$\mathcal{H} = \begin{bmatrix} E_1 & 0 & H_{13} & H_{13}^* \\ 0 & E_2 & H_{23} & -H_{23} \\ H_{13}^* & H_{23}^* & E_3 & H_{33} \\ H_{13} & -H_{23} & H_{33} & E_3 \end{bmatrix} \tag{34}$$

where

$$\left.\begin{aligned} E_1 &= \Delta + \gamma_1 \Gamma + \frac{1}{2}\gamma_5 \Gamma^2 \\ E_2 &= \Delta - \gamma_1 \Gamma + \frac{1}{2}\gamma_5 \Gamma^2 \\ E_3 &= \frac{1}{2}\gamma_2 \Gamma^2 \end{aligned}\right\} \tag{35}$$

and

$$\Gamma = 2 \cos \pi\xi \tag{36}$$

where ξ is the coordinate along k_z measured from the point K in the Brillouin zone as shown in figure 5. Figure 5 shows the Fermi surface which is located along the Brillouin zone edges HKH (ref. 2). Whether the charge carriers at A and B are electron or hole (one must be electron, the other hole) is associated with the signs of the band parameters. These parameters are γ_0, γ_1, γ_2, γ_3, γ_4, γ_5, Δ, and ε_F, which

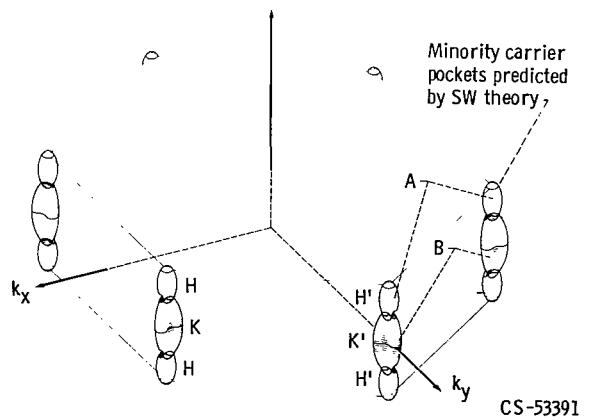

Figure 5. - Brillouin zone of graphite. Fermi surfaces along H, K, H are labeled A and B.

can be determined from experiment. Magnetoreflection and deHaas - van Alphen experiments have given the best values so far (ref. 23).

$$\left.\begin{aligned}
\gamma_0 &= 2.85\pm0.10 \text{ eV} \\
\gamma_1 &= 0.31\pm0.02 \text{ eV} \\
\gamma_2 &= -0.0185 \text{ eV} \quad \leftarrow \\
\gamma_3 &= +0.29\pm0.02 \text{ eV} \\
\gamma_4 &= +0.18\pm0.02 \text{ eV} \quad \leftarrow \\
\gamma_5 &= -0.0185 \text{ eV} \quad \leftarrow \\
\Delta &= +0.009 \text{ eV} \quad \leftarrow \\
\mathcal{E}_F &= -0.022 \text{ eV} \quad \leftarrow
\end{aligned}\right\} \tag{37}$$

The signs of these coefficients were determined by Schroeder et al. (ref. 6), and the constants with arrows change sign if the assignment of electrons and holes is reversed (see fig. 5). A direct and independent determination of signs is made from the results of the present experiments as will be discussed in the section "Consequences of Electron and Hole Carrier Assignment to the Energy Band Structure."

The γ_3 factor distorts the Fermi surfaces from having circular cross section perpendicular to the "C" axis. However, this has little effect on the extremal cross sectional areas or effective masses. Consequently, γ_5 will be ignored (set equal to zero) in any later discussion involving the band parameters.

In zero magnetic field the energy bands are described, neglecting γ_3, by

$$\left.\begin{aligned}
\mathcal{E} &= \frac{1}{2}(E_1 + E_2) \pm \left[\frac{1}{4}(E_1 - E_3)^2 + \gamma_0^2(1 - \nu)^2\sigma^2\right]^{1/2} \\
\mathcal{E} &= \frac{1}{2}(E_2 + E_3) \pm \left[\frac{1}{4}(E_2 - E_3)^2 + \gamma_0^2(1 + \nu)^2\sigma^2\right]^{1/2}
\end{aligned}\right\} \tag{38}$$

where E_1, E_2, and E_3 are given by equation (35). The radial coordinate, centered on the HKH edge, for directions perpendicular to k_z is given by σ, and ν is given by

$$\nu = \frac{\gamma_4 \Gamma}{\gamma_0} \tag{39}$$

where Γ is defined by equation (36).

In figure 6 energy (from eqs. (35) and (38) is plotted as a function of the coordinate ξ along the k_z direction for $\sigma = 0$. On the left in figure 6 the bands are plotted with the old signs (negative of those indicated by arrows in eq. (37)). On the right in figure 6 the signs are those indicated in equation (37). Figure 6 also shows that $\mathcal{E}_F$ is measured from the bottom (old notation) or top (new notation) of the conduction band at points H.

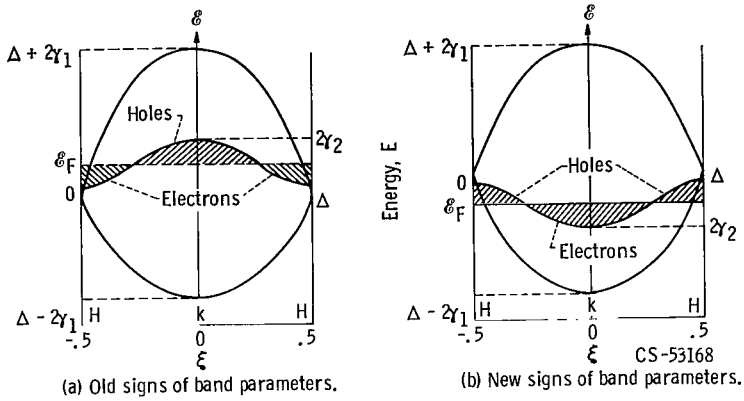

(a) Old signs of band parameters.

(b) New signs of band parameters.

Figure 6. - Energy bands for graphite against the ξ coordinate along k (from eq. (35)).

The relation between the band parameters and the extremal cross sectional area of the Fermi surface at the center of the zone edge (point K in fig. 5) is

$$A_K = \frac{4\pi(1 + \nu)^2}{3a_0^2\gamma_0^2} (2\gamma_2 - \mathcal{E}_F)(\Delta - 2\gamma_1 + 2\gamma_5 - \mathcal{E}_F) \tag{40}$$

and the effective mass at the center of the edge is

$$m_K^* = - \frac{4\hbar^2(1 + \nu)^2}{3a_0^2\gamma_0^2} \left(\frac{1}{2}\Delta + \gamma_1 + \gamma_2 + \gamma_5 - \mathcal{E}_F\right) \tag{41}$$

With spin-orbit interaction included in the Hamiltonian, the tips of the "A" Fermi surface sections shown in figure 5 break into a separate tiny pocket of carriers located at H as marked. The extremal cross sectional area A_m of this surface, perpendicular to the k_z direction is predicted (ref. 2) to be

$$A_m = \frac{4\pi\mathcal{E}_F(\mathcal{E}_F - \Delta)}{3a_0^2\gamma_0^2} \tag{42}$$

For a magnetic field present the energy levels were derived by McClure (ref. 24) and Inoue (ref. 25) from SW theory. For $\gamma_3 = 0$ the Hamiltonian in a field has matrix elements given by

$$\mathcal{H} = \begin{bmatrix} E_1 & 0 & H'_{13} & H'_{14} \\ 0 & E_2 & H'_{23} & H'_{24} \\ H'_{13} & H'_{23} & E_3 & 0 \\ H'_{14} & H'_{24} & 0 & E_3 \end{bmatrix} \tag{43}$$

where E_1, E_2, and E_3 are given by equation (35) and

$$\left.\begin{aligned} H'_{13} &= -\left(\frac{Q}{2}\right)^{1/2}(1-\nu)(n+1)^{1/2} \\ H'_{14} &= -\left(\frac{Q}{2}\right)^{1/2}(1-\nu)n^{1/2} \\ H'_{23} &= \left(\frac{Q}{2}\right)^{1/2}(1+\nu)(n+1)^{1/2} \\ H'_{24} &= -\left(\frac{Q}{2}\right)^{1/2}(1+\nu)n^{1/2} \\ Q &= 3a_0^2\gamma_0^2\frac{eH}{2\hbar C} \end{aligned}\right\} \tag{44}$$

and a_0 is a lattice constant equal to 2.456×10^{-8} centimeter. The secular equation from equation (43) is

$$\left(n+\frac{1}{2}\right)Q = \frac{E-E_3}{2}\left[\frac{E-E_1}{(1-\nu)^2}+\frac{E-E_2}{(1+\nu)^2}\right] \pm \left(\left\{\frac{E-E_3}{2}\left[\frac{E-E_1}{(1-\nu)^2}-\frac{E-E_2}{(1+\nu)^2}\right]\right\}^2+\frac{Q^2}{4}\right)^{1/2} \tag{45}$$

EXPERIMENTAL

Three different magnets were used for the present investigations: an 18.5-tesla (1 T = 10 kG) liquid-neon-cooled steady state solenoid (ref. 26), a 10.5-tesla superconducting solenoid, and a 4.0-tesla transverse split pair superconducting magnet. The last magnet was used when measuring thermoelectric power as a function of angle between the magnetic field and the graphite C axis. For the 10.5- and 4.0-tesla magnets, field measurements were accurate to within 0.2 percent. The samples were highly ordered pressure annealed pyrolytic graphite. The distribution of directions of "C" axes of the various crystallites was measured by X-ray scattering to be on the order of 2^{o}. Transmission electron microscope studies found typical grain size to be about 10-micrometer diameter. The ratio of electrical resistance at 300 K to that at 4.2 K was 1.5 for sample PG 3, 9 for PG 4, and 9.5 for PG 5. By comparison, natural single crystals have had ratios ranging from 12 to 37 (ref. 3).

The sample geometry is shown in figure 7. For ρ_{yy} and ρ_{yx} measurements, electric current flows along the sample length (±y direction) perpendicular to the field

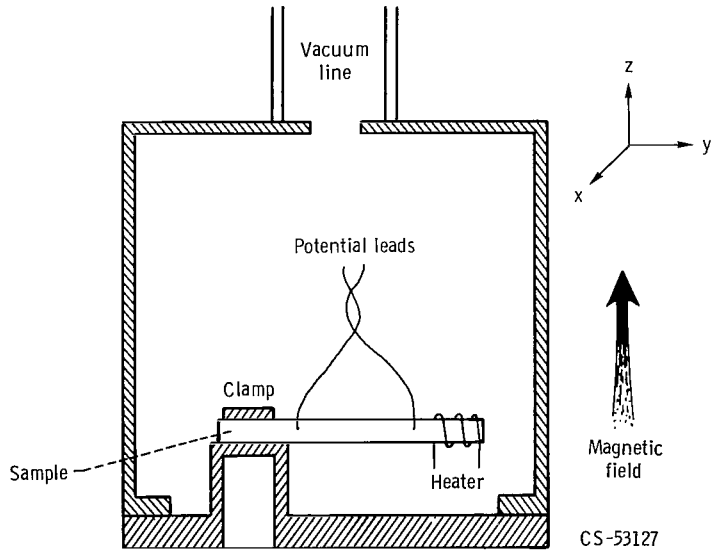

Figure 7. - Experimental geometry. Coordinate system defines components of tensors; z direction defined by field; y direction defined by sample length and current flow.

and voltages are recorded. The measured electric fields are $\overline{E}^*$, and from equation (3)

$$\overline{E}^* = \hat{\rho}\overline{J} \tag{46}$$

when there are no temperature gradients. For adiabatic thermopower ϵ'_{yy} and Nernst-Ettingshausen ϵ'_{xy} measurements, a constant heat flow $\overline{w}^*$ is maintained in the sample and equation (1) shows

$$\overline{E}^* = \epsilon'\overline{w}^* \tag{47}$$

To measure the thermal resistivity tensor components, equation (8) is used

$$\overline{G} = \hat{\gamma}\overline{w}^* \tag{8}$$

where $\overline{G}$ is the negative temperature gradient vector. To calculate the tensor elements of the isothermal thermopower $\hat{\epsilon}$, we use equation (10) to obtain $\hat{\lambda}$ from $\hat{\gamma}$ and equation (11) to obtain ϵ from $\hat{\epsilon}'$.

Voltages are measured with a direct-current nanovoltmeter and recorded against field or angle on an x-y recorder. Temperature gradients are measured with an alternating-current Wheatstone bridge. Evanohm is used for heater wire to supply the constant heat current $\overline{w}^*$. The power from an Evanohm heater was shown to change by less than 2 percent in going from 0 to 18.5 tesla (ref. 27).

EXPERIMENTAL RESULTS

Magnetoresistance

In figure 8 the magnetoresistance ρ_{yy} and Hall resistivity ρ_{yx} are plotted as a function of field to 10 tesla (1 T = 10 kG) at 1.1±0.05 K. We find experimentally that $\rho_{yx} << \rho_{yy}$ and that quantum oscillations are obvious in both quantities. Using equation (12) for fields parallel to the high symmetry C axis

$$\sigma_{yy} = \frac{\rho_{yy}}{\rho_{yy}^2 + \rho_{yx}^2} \approx \frac{1}{\rho_{yy}} \tag{48}$$

Thus maxima predicted by equation (13) for σ_{yy} result in minima for ρ_{yy} when Landau levels coincide with the Fermi energy. Since

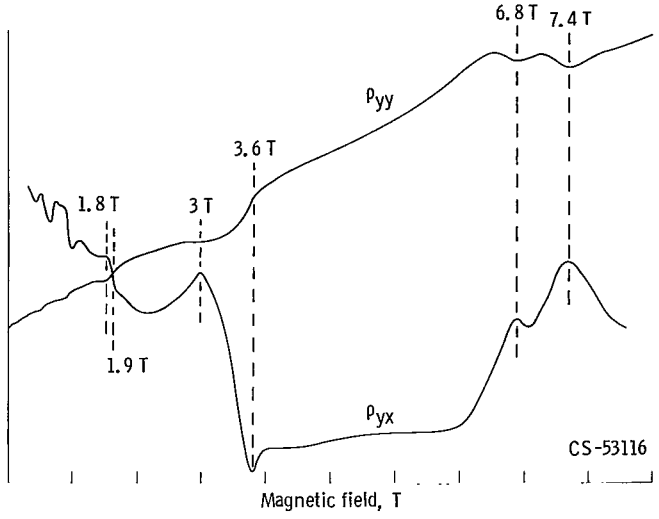

Figure 8. - Hall resistivity ρ_{yx} and magnetoresistance ρ_{yy} as functions of field at 1.1 K. Sample PG 5; scales are not the same.

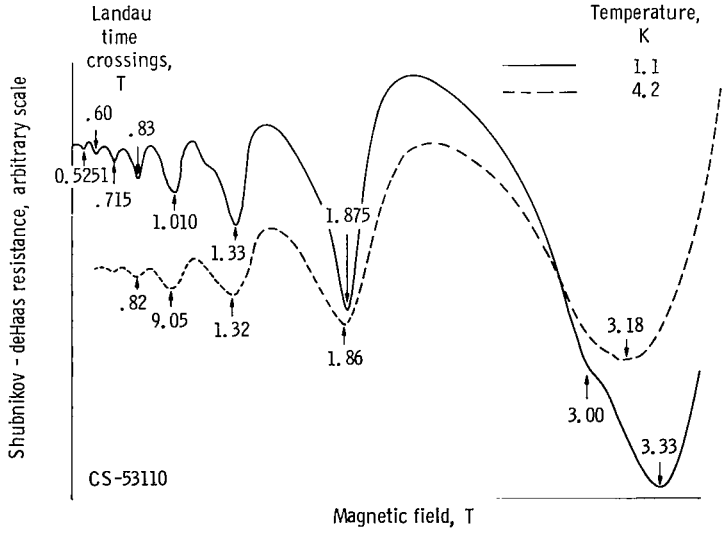

Figure 9. - Oscillatory part of magnetoresistance as function of field at 4.2 and 1.1 K.

$$\sigma_{yy} \simeq \frac{1}{\rho_{yy}}$$

$$\tilde{\rho}_{yy} \propto \frac{\tilde{\sigma}_{yy}}{\left(\sigma^{o}_{yy}\right)^2} \tag{49}$$

where $\tilde{\rho}_{yy}$ means the oscillatory part of the resistivity. From equation (16) for the oscillatory conductivity

$$\tilde{\rho}_{yy} \propto \rho^{o}_{yy}\left(\frac{\hbar\omega}{\mathcal{E}_F}\right)^{1/2} \sum_{M} \frac{2\pi^2 MkT}{\hbar\omega}\left(\sinh\frac{2\pi^2 MkT}{\hbar\omega}\right)^{-1}(2\pi M)^{-1/2}\cos\left(\frac{2\pi MF}{H} - \frac{\pi}{4} - \pi M\right) \tag{50}$$

In figure 9 experimental results of the oscillatory part of the resistivity is plotted as a function of field to 4 tesla. At 4.2 K the oscillations are undistorted up to nearly 2 tesla, and the oscillations are described by the $M = 1$ term in equation (50) for low fields. At 1.1 K the oscillations are spike shaped and the minima shifted to higher fields. It takes more than the $M = 1$ term in equation (60) to describe the oscillations. In the limit of near zero temperature and near perfect crystals, the resistance minima would be very sharp and drop nearly to zero as follows from equation (13).

TABLE I. - COMPARISON OF HOLE MAJORITY CARRIER EXTREMA FOR LANDAU LEVEL CROSSING OF ϵ_F WITH PREDICTIONS OF SUGIHARA AND ONO (REF. 11)

Landau level	Theoretical field position (Sugihara and Ono)	Thermopower maxima	Resistance minima	Conductivity, σ_{xy} minima
	Field, T			
1	3.6	3.66±0.02	3.33±0.02	3.64±0.1
2	1.99	1.97±0.03	1.88±0.02	1.94±0.04
3	1.42	1.39±0.01	1.36±0.02	1.39±0.02
4	1.10	1.08±0.02	1.01±0.02	1.11±0.05
5	----	.88±0.02	.83±0.02	.86±0.03
6	----	.75±0.03	.72±0.03	.75±0.03
7	----	.64±0.03	.60±0.03	.63±0.02

TABLE II. - COMPARISON OF ELECTRON MAJORITY CARRIER EXTREMA FOR LANDAU LEVEL CROSSING OF ϵ_F WITH PREDICTIONS OF SUGIHARA AND ONO (REF. 11)

Landau level	Theoretical field position (Sugihara and Ono)	Thermopower minima	Resistance minima	Conductivity, σ_{xy} maxima
	Field, T			
1	6.4	[a]$_{7.0}$ 7.68±0.05 6.92±0.05	[a]$_{7.2}$ 7.6±0.1 6.8±0.1	[a]$_{7.1}$ 7.4±0.1 6.8±0.1
2	2.95	2.98±0.02	3.0±0.05	3.0±0.05
3	1.95	---	---	1.86±0.02
4	1.54	---	---	1.50±0.02
5	----	---	---	1.22±0.02

[a]Spin split Landau level.

The field values for resistivity minima occurring at coincidence of $\mathcal{E}_F$ and Landau levels are predicted by Sugihara and Ono (ref. 11). These are listed in tables I and II for the quantum numbers n for the hole carriers and electron carriers, respectively. The resistivity minima from figure 9 for 1.1 K are also listed. As expected from the theory (IB) the resistance minima occur at slightly lower fields than Landau level crossings. Included in the table are the minima near 7 tesla shown in figure 8. At 1.1 K the weak $n = 2$ minima due to the electron carriers is visible (figs. 8 and 9) at 3 tesla. The double minima near 7 tesla for the $n = 1$ electron carriers is double due to spin splitting of the Landau levels. This splitting will be discussed in the section "Spin Splitting." The deHaas - van Alphen period of the minima in figure 9 is 0.206±0.005 tesla^{-1}.

Hall Coefficient

Figure 10 shows a plot of resistivity ρ_{yy}, Hall resistivity ρ_{yx}, and Hall conductivity times H^2, calculated from ρ_{yy} and ρ_{yx} using equation (12). The positions of extrema in all three quantities are marked by field value and Landau quantum number. As discussed previously Argyres (ref. 8) predicts that maximal extrema will result in σ_{xy} when Landau levels for electron carriers cross $\mathcal{E}_F$, and minimal extrema will result when hole levels cross $\mathcal{E}_F$. In figure 10, $\sigma_{xy}H^2$ is plotted rather than σ_{xy} in order to best observe extrema, and has (spin split) maxima at 7 tesla, and maxima at 3.0 and 1.8 tesla. This series of extrema is thus due to electron carriers. $\sigma_{xy}H^2$ has

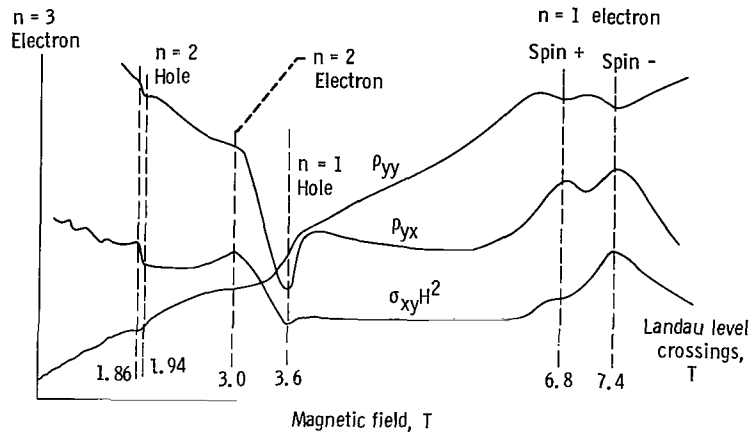

Figure 10. - Representative data for Hall resistivity, magneto-resistance and Hall conductivity as function of field at 1.1 K. Sample PG 5.

minima at 3.64 and 1.94 tesla, and this series is due to hole carriers. The field values correspond to crossings of Landau levels predicted by Sugihara and Ono (ref. 11) and these are listed in table I for holes, and table II for electrons.

In figure 11 the measured ρ_{yx} is plotted as a function of field at 1.1 K. A complicated series of superimposed maxima and minima is observed at low fields. A few of the extrema are marked by field and quantum number in figure 11. The best values from all data including figure 11 for these extrema are also listed in tables I and II.

By comparing the σ_{xy} extrema with resistance minima and Sugihara and Ono predictions, we find that σ_{xy} minima belong to the deHaas - van Alphen series with period 0.205 ± 0.005 tesla^{-1}. Soule, McClure, and Smith (ref. 3) (SMS) have shown that this

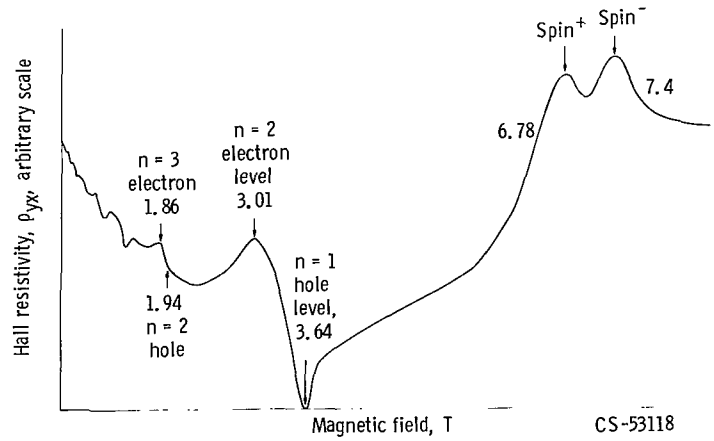

Figure 11. - Representative data for Hall resistivity as function of field at 1.1 K showing low field detail in sample PG 5 and spin splitting near 7 tesla.

deHaas-van Alphen period belongs to the Fermi surface section marked "A" in figure 5. This frequency assignment is also predicted by the SW band structure theory. Thus the Fermi surface sections at "A" in figure 5 are hole type carriers.

The σ_{xy} maxima, when compared with Sugihara and Ono predictions (table II) are part of the deHaas - van Alphen series with period 0.16 ± 0.01 tesla^{-1} and located at "K" in the Brillouin zone (fig. 5). The Fermi surface section B in figure 5 is thus the electron section. Sugihara and Ono theory and experiment are in accord for all data except for the $n = 1$ (spin split) electron level near 7 tesla.

The major conclusions from the magnetoresistance and Hall effect results are:

(1) The carriers marked A in figure 5 are holes and those marked B are electrons.

(2) The Sugihara and Ono theory is within experimental uncertainty except for the $n = 1$ electron level which is found higher in field than predicted.

(3) The Adams and Holstein theory for resistance in strong magnetic fields is qualitatively correct in predicting (a) sharp maxima at low temperatures for σ_{yy}, (b) maxima shift to higher field values as the temperature decreases, and (c) resistance minima (conductivity maxima) for both electron and hole carriers.

Thermoelectric Power and Thermal Conductivity

The adiabatic coefficient are experimentally measured, but the isothermal coefficients from equation (1) with $J = 0$ must be calculated in order to compare with theory.

$$\overline{E}^* = \hat{\epsilon}' \overline{w}^* \tag{51}$$

so with $\overline{w}^*$ in the y direction

$$E_y = \epsilon'_{yy} w_y \tag{52}$$

and

$$E_x = \epsilon'_{xy} w_y \tag{53}$$

(For relative coordinates see fig. 7.) The magnetic field is maintained along the z direction. From equations (52) and (53), a measurement of E_y with constant w_y gives ϵ'_{yy} the adiabatic thermopower, and E_x gives ϵ'_{yx} the adiabatic Nernst-Ettingshausen coefficient. To obtain the isothermal $\hat{\epsilon}$ tensor we use

$$\hat{\epsilon} = \hat{\epsilon}' \hat{\lambda} \tag{11}$$

and

$$\hat{\lambda} = \hat{\gamma}^{-1} \tag{54}$$

where $\hat{\gamma}$ is the thermal resistivity tensor. For fields along the C axis of graphite

$$\hat{\gamma} = \begin{pmatrix} \gamma_{yy} & \gamma_{xy} & 0 \\ -\gamma_{xy} & \gamma_{yy} & 0 \\ 0 & 0 & \gamma_{zz} \end{pmatrix} \tag{55}$$

and

$$\lambda_{yy} = \frac{\gamma_{yy}}{\gamma_{yy}^2 + \gamma_{xy}^2} \tag{56}$$

$$\lambda_{yx} = \frac{\gamma_{xy}}{\gamma_{yy}^2 + \gamma_{xy}^2} \tag{57}$$

Experimentally we find $\gamma_{xy} << \gamma_{yy}$ for all ranges of magnetic field. Thus

$$\lambda_{yy} \simeq \frac{1}{\gamma_{yy}} \tag{58}$$

and

$$\lambda_{yx} \simeq \frac{\gamma_{xy}}{\gamma_{yy}^2} << \lambda_{yy} \tag{59}$$

The amplitude of Nernst-Ettingshausen coefficient oscillations were up to eight times larger than the thermopower. However, γ_{xy} was smaller than γ_{yy} divided by 50.

Equation (10) shows that

$$\hat{\gamma} = \hat{\lambda}^{-1} \tag{10}$$

where symmetry makes $\gamma_{xx} = \gamma_{yy}$, $\gamma_{xy} = -\gamma_{yx}$, and $\gamma_{xz} = \gamma_{yz} = \gamma_{zx} = \gamma_{zy} = 0$. Since $\gamma_{yy} \geq 50\ \gamma_{xy}$ it follows from equations (10) and (11) that

$$\epsilon_{yy} \approx \epsilon'_{yy}\lambda_{yy} \tag{60}$$

and from equation (58)

$$\epsilon_{yy} \simeq \frac{\epsilon'_{yy}}{\gamma_{yy}} \tag{61}$$

We have measured γ_{yy} as a function of field to 10 tesla and find that it saturates to a constant value after increasing for about 0.1 to 0.2 tesla. This saturation is due to a freezing out of thermal conduction by electrons. As the field increases, conductivity by electrons decreases until it is unimportant compared with lattice conduction. Lattice conduction is independent of field. We did find very weak quantum oscillations in the thermal resistivity in the saturation region of magnetic field. These were in phase with the electrical resistivity oscillations, so were attributed to remnant electronic conductivity and not to the phenomenon of phonon scattering from quantized electron states (ref. 28).

Since γ_{yy} is independent of field, equation (61) shows that

$$\epsilon_{yy}(H) \propto \epsilon'_{yy}(H) \tag{62}$$

at a fixed temperature. Thus measurements of ϵ'_{yy} as a function of field are proportional to ϵ_{yy} as a function of field. In Ziman's (ref. 13) notation for Thermopower, S_{yy} (see eq. (22)),

$$S_{yy} = -\epsilon_{yy} \tag{63}$$

In figure 12 the thermoelectric power of sample PG 3 is plotted as a function of magnetic field to 2.4 tesla at 1.2 K. This figure shows that at low fields a very small frequency oscillation (minority carriers) is superimposed on the larger frequency (majority carrier) oscillations. These oscillations could possibly result from carriers near the Brillouin zone boundary at points "H" shown in figure 5. In figure 12 the minima in thermopower for the majority carrier oscillations are marked by arrows.

In sample PG 3 (resistance ratio 1.5) we studied the oscillation periods (P = 1/F). For the electron carriers the deHaas - van Alphen period is 0.155 ± 0.005 tesla^{-1} for field parallel to the C axis. These oscillation periods were studied over a wide range of angle between the field and the C axis and dominated at low field and low temperature. At 4.2 K, oscillations from the hole Fermi surface dominated. Parallel to the C axis this period was 0.208 ± 0.008 tesla^{-1}. In figure 13 the electron and hole (majority carrier) periods are plotted as a function of angle out to 70° to 80° from C. The solid lines are from the natural single crystal data of Soule, McClure, and Smith (ref. 3). The electron (lower curve) period found in PG 3 was slightly higher than the Soule, McClure, and Smith results but experimental errors overlap. The period against angle data of figure 13 is characteristic of a nearly cylindrical Fermi surface, and Soule, McClure, and

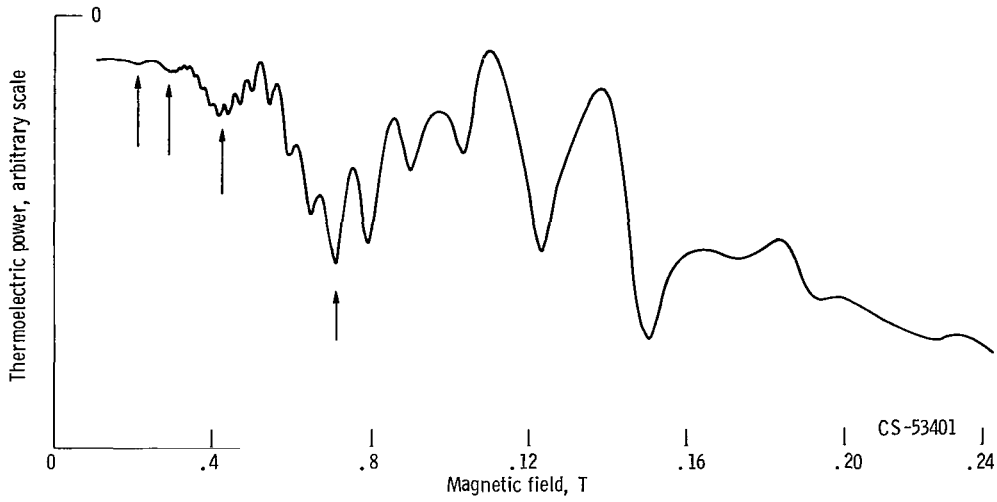

Figure 12. - Thermopower S_{yy} as function of field at 1.1 K. Two carrier oscillations: majority electrons and minority carriers. Sample PG 3.

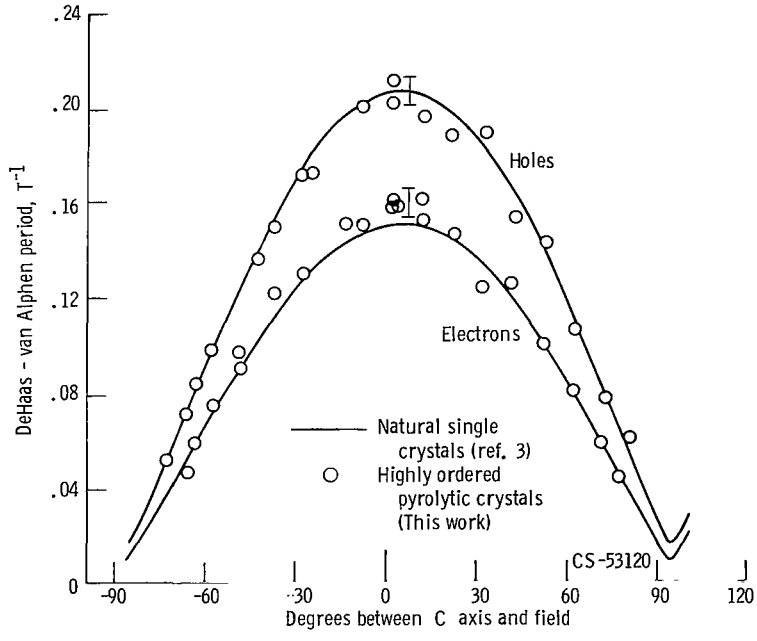

Figure 13. - deHaas - van Alphen period P as function of angle between field and C axis. Majority carriers in sample PG 3.

Smith found the ratio of areas for the hole surface in natural single crystals to be

$$\frac{A(90^{o})}{A(0^{o})} = 12.1 \tag{64}$$

where $A(0^{o})$ is the extremal cross sectional area of the Fermi surface for a field parallel to the C-axis and $A(90^{o})$ is for a field perpendicular to C. Within experimental error we find that natural single crystals and pyrolytic graphite have identical areas for both electrons and holes out to $\pm 70^{o}$ from the C-axis.

In figure 14 the deHaas - van Alphen frequency is plotted against the angle between the magnetic field and the C-axis for the same data as appear in figure 13. The frequency is proportional to the extremal cross-sectional area of the Fermi surface perpendicular to the field. Figure 14 demonstrates how little change in area occurs for angles less than $\pm 40^{o}$ from C. From 60^{o} to 90^{o} the change in area is very rapid.

In figure 15 the thermoelectric power of sample PG 4 (resistance ratio, 9) is plotted as a function of field to 10 tesla. The field values for electron and hole extrema are marked, as well as the quantum numbers associated with each peak. In the theory section, it was concluded that sharp positive peaks result from hole carrier Landau levels crossing $\mathcal{E}_F$. The series 3.63 tesla, 1.96 tesla, etc., are thus due to hole Landau levels crossing $\mathcal{E}_F$. They have a deHaas - van Alphen period of 0.206 ± 0.007 tesla^{-1}. As discussed earlier, this period originates from the Fermi surface section marked A in figure 5. The A surface is thus a hole surface. The minima seen in figure 12 at 7 tesla (spin split) are due to electron Landau levels crossing $\mathcal{E}_F$ and show that the Fermi surface B in figure 5 is for electrons. This assignment of electrons and holes agrees with out Hall results. We have thus provided two independent and direct experiments to confirm the assignment of electrons and holes in the Brillouin zone. This assignment agrees with the results of Schroeder, Dresselhaus, and Javan (ref. 7).

In figure 16 the thermopower of sample PG 5 (resistance ratio, 9.5) is plotted as a function of field to 4 tesla. These data are the sharpest of the three samples. The same assignment of electrons and holes in the Brillouin zone results as with PG 4. An interesting part of these data is the line shape of the oscillations. The trace, as a function of increased field, rises rapidly and plateaus coming down the high field side. The thermodynamic theory predicts the plateauing first and the sharp drop on the high field side as shown in figure 3. The same is true for the theories presented in references 18 to 20. However, Horton (ref. 14) predicts the observed line shape, as shown in figure 14. This lends support to the Horton theory.

The observed spikes in thermopower occur at fields close to those predicted by Sugihara and Ono. The one exception is the spin split $n = 1$ electron level centered near 7 tesla. This peaks at a higher field than predicted. All of the observed crossings

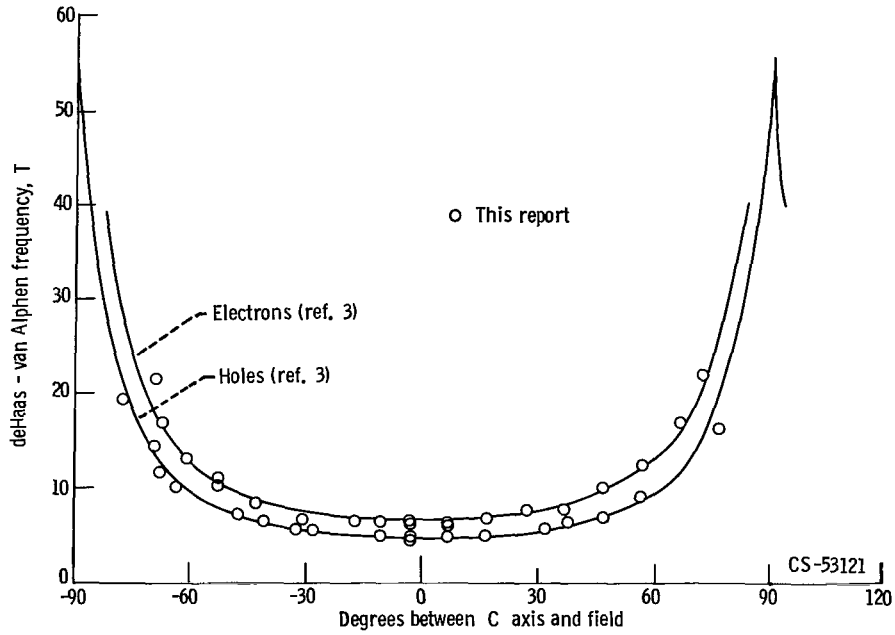

Figure 14. - deHass - van Alphen frequency as function of angle between field and C axis. Majority carriers in sample PG 3.

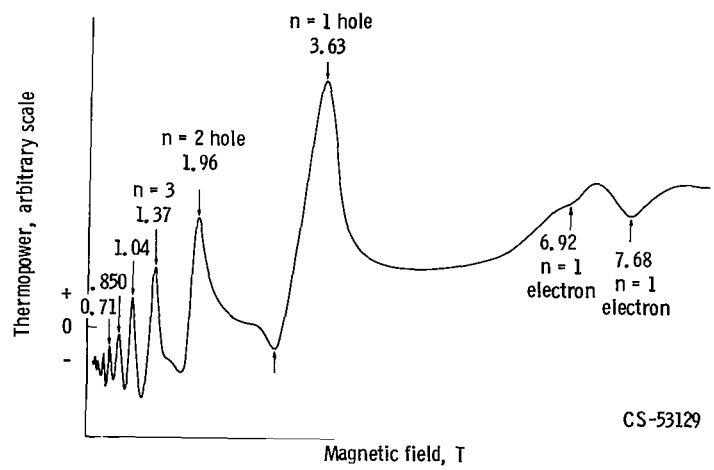

Figure 15. - Thermopower against field at 1.1 K for PG 4. Landau level crossings for both electrons (spin split) and hole carriers marked.

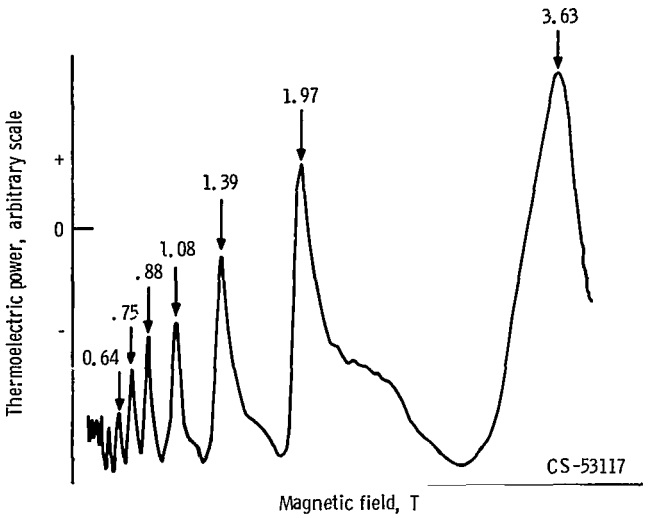

Figure 16. - Thermopower as function of field at 1.1 K for sample PG 5.

of Landau levels at $\mathcal{E}_F$ are listed in tables I and II and compare favorably with Sugihara and Ono theory.

Consequences of Electron and Hole Carrier Assignment to the Energy Band Structure

Previous to the work of Schroeder, Dresselhaus, and Javan (ref. 7), the energy bands were as shown on the left in figure 6. The parameters γ_2, γ_5, and $\mathcal{E}_F$ were positive, and γ_4 and Δ were negative. As shown on the right in figure 6, when electrons are located near the center of the zone edge ($\xi = 0$), the coefficients γ_2 and $\mathcal{E}_F$ reverse sign. Our quantum Hall effect, and thermoelectric power results confirm that holes are at A and electrons are at B, as shown in figure 5. This makes γ_2 and $\mathcal{E}_F$ negative. From equation (35) E_3 then has negative values. The McClure-Inoue (refs. 24 and 25) equation

$$\left(n + \frac{1}{2}\right)Q = \frac{E - E_3}{2}\left[\frac{E - E_1}{(1-\nu)^2} + \frac{E - E_2}{(1+\nu)^2}\right] \pm \left(\left\{\frac{E - E_3}{2}\left[\frac{E - E_1}{(1-\nu)^2} - \frac{E - E_2}{(1+\nu)^2}\right]\right\}^2 + \frac{Q^2}{4}\right)^{1/2} \tag{45}$$

can still be satisfied if the signs of Δ, γ_4, and γ_5 are reversed. From equation (35),

$$\left.\begin{aligned} E_1 &= \Delta + \gamma_1\Gamma + \frac{1}{2}\gamma_5\Gamma^2 \quad \text{becomes } -E_2 \\ E_2 &= \Delta - \gamma_1\Gamma + \frac{1}{2}\gamma_5\Gamma^2 \quad \text{becomes } -E_1 \\ E_3 &= \frac{1}{2}\gamma_2\Gamma^2 \quad \text{becomes } -E_3 \end{aligned}\right\} \tag{65}$$

In equation (45) replace E_1 by $-E_2$, E_2 by $-E_1$, E_3 by $-E_3$, and E by -E, and the equation is unchanged. Equation (40) for the cross sectional area predicts the same area in both assignments of sign. Equation (41) for the effective mass is also unchanged in value by the sign change.

Spin Splitting

Spin splitting of the $n = 1$ electron Landau levels are observed in the magnetoresistance (figs. 8 and 10), the Hall coefficient (figs. 8, 10, and 11), and the thermopower (fig. 15). For all of these, the separation of peaks is between 0.6 and 0.7 tesla. This is further confirmed by the observation of very nearly the same magnitude for splitting in three different pyrolytic graphite samples. In a natural single crystal, we have recently observed splittings in the $n = 1$ and $n = 2$ electron levels and in the $n = 1$ hole level. A study of consequences of the spin splitting is discussed in a separate paper (ref. 29).

CONCLUSIONS

The major findings of this study are

1. Carriers marked A in figure 5 are holes and those marked B are electrons. This assignment is made from Hall effect and independently from the thermopower quantum resonances.

2. The theory of Sugihara and Ono is within experimental uncertainty of predicting the observed positions of Landau level crossings of ε_F. The one exception is the $n = 1$ electron level, which is found higher in field than predicted.

3. The Adams and Holstein theory for resistance of a degenerate conductor in a strong magnetic field, is correct in predicting sharp maximas for σ_{yy} at coincidence of a Landau level and the Fermi energy for both electron and hole type carriers. Shifts of peaks to lower fields at higher temperatures is observed.

4. A thoery by Horton appears to predict the correct line shape of quantum oscilla-

tions in the thermopower at high fields. A Dingle temperature of 1.5 K gives a good fit between Horton theory and experiment. Other theories were found not to satisfactorily explain experimentally observed wave shapes.

5. We have made the first observation of spin splitting of Landau levels in graphite. The $n = 1$ electron Landau level is spin split by 0.6 to 0.7 tesla at 7 tesla. This provides a measure of the spin orbit splitting at the point K in the center of the Brillouin zone edge.

6. The thermal resistivity saturates to a constant value independent of magnetic field strength for fields above about 0.2 tesla.

7. Pyrolytic and natural single crystals produce the same deHaas - van Alphen frequencies as a function of angle between the field and the C axis. This lends support to the use of the single crystal band theory for pyrolytic samples.

8. A low deHaas - van Alphen frequency (minority carrier) oscillation is observed which could possibly originate from carriers in the points H in the Brillouin zone.

Lewis Research Center,
National Aeronautics and Space Administration,
Cleveland, Ohio, June 18, 1970,
129-02.

REFERENCES

1. Moore, A. W.; Ubbelohde, A. R.; and Young, D. A.: Stress Recrystallization of Pyrolytic Graphite. Proc. Roy. Soc. (London), Ser. A, vol. 280, no. 1381, July 21, 1964, pp. 153-169.

2. Williamson, S. J.; Foner, S.; and Dresselhaus, M. S.: deHaas - van Alphen Effect in Pyrolytic and Single-Crystal Graphite. Phys. Rev., vol. 140, no. 4A, Nov. 15, 1965, pp. 1429-1447.

3. Soule, D. E.; McClure, J. W.; and Smith, L. B.: Study of the Shubnikov-deHaas Effect. Determination of the Fermi Surfaces in Graphite. Phys. Rev., vol. 134, no. 2A, Apr. 20, 1964, pp. 453-470.

4. Dresselhaus, Mildred S.; and Mavroides, John G.: Magnetoreflection Experiments in Graphite. Carbon, vol. 1, no. 3, 1964, pp. 263-268.

5. Slonczewski, J. C.; and Weiss, P. R.: Band Structure of Graphite. Phys. Rev., vol. 109, no. 2, Jan. 15, 1958, pp. 272-279.

6. Soule, D. E.: Change in Fermi Surfaces of Graphite by Dilute Acceptor Doping. IBM J. Res. Dev., vol. 8, no. 3, July 1964, pp. 268-273.

7. Schroeder, P. R.; Dresselhaus, M. S.; and Javan, A.: Location of Electron and Hole Carriers in Graphite from Laser Magnetoreflection Data. Phys. Rev. Letters, vol. 20, no. 23, June 3, 1968, pp. 1292-1295.

8. Argyres, Petros N.: Quantum Theory of Transport in a Magnetic Field. Phys. Rev., vol. 117, no. 2, Jan. 15, 1960, pp. 315-328.

9. Wagoner, G.: Spin Resonance of Charge Carriers in Graphite. Phys. Rev., vol. 118, no. 3, May 1, 1960, pp. 647-653.

10. Adams, E. N.; and Holstein, T. D.: Quantum Theory of Transverse Galvanomagnetic Phenomena. J. Phys. Chem. Solids, vol. 10, no. 4, 1959, pp. 254-276.

11. Sugihara, Kô; and Ono, Shûsuke: Galvanomagnetic Properties of Graphite at Low Temperatures. J. Phys. Soc. Japan, vol. 21, no. 4, Apr. 1966, pp. 631-637.

12. Woollam, John A.: Thermomagnetic Effects and Fermi-Surface Topology: Results in Metallic Tin at Low Temperatures. Phys. Rev., vol. 185, no. 3, Sept. 15, 1969, pp. 995-1002.

13. Ziman, J. M.: Electrons and Phonons. Clarendon Press, Oxford, 1960.

14. Horton, Philip B.: Quantum Transport Theory of Free Electrons in a Strong Magnetic Field. Ph.D. Thesis, Louisiana State Univ., 1964.

15. Fair, Gale; and Taylor, P. L.: Theory of Thermomagnetic Transport Coefficients in an Anisotropic Metal. Bull. Am. Phys. Soc., vol. 15, no. 3, Mar. 1970, p. 252.

16. Callen, Herbert B.: The Application of Onsager's Reciprocal Relations to Thermoelectric, Thermomagnetic, and Galvanomagnetic Effects. Phys. Rev., vol. 73, no. 11, June 1, 1948, pp. 1349-1358.

17. MacDonald, David K. C.: Thermoelectricity: An Introduction to the Principles. John Wiley & Sons, Inc., 1962, p. 11.

18. Obraztsov, Yu. N.: The Thermal EMF of Semiconductors in a Quantizing Magnetic Field. Soviet Phys.-Solid State, vol. 7, no. 2, Aug. 1965, pp. 455-461.

19. Zyryanov, P. S.; and Kalashnikov, V. P.: Quantum Theory of the Thermomagnetic Effects in Metals and Semiconductors. Phys. Metals Metallography, vol. 18, no. 2, 1964, pp. 8-13.

20. Tsĕndin, K. D.; and Éfros, A. L.: Theory of Thermal EMF in a Quantizing Magnetic Field in the Kane Model. Soviet Phys.-Solid State, vol. 8, no. 2, Feb. 1966, pp. 306-308.

21. Lifshitz, I. M.; and Kosevich, A. M.: Theory of Magnetic Susceptibility in Metals at Low Temperatures. Soviet Phys.-JETP, vol. 2, no. 4, July 1956, pp. 636-645.

22. Dingle, R. B.: Some Magnetic Properties of Metals. II. The Influence of Collisions on the Magnetic Behaviour of Large Systems. Proc. Roy. Soc. (London), Ser. A, vol. 211, no. 1107, Mar. 20, 1952, pp. 517-525.

23. Schroeder, P. R.; Dresselhaus, M. S.; and Javan, A.: High Resolution Magneto-spectroscopy of Graphite. Presented at the American Physical Society Conference on the Physics of Semimetals and Narrow Gap Semiconductors, Dallas, Texas, Mar. 20-21, 1970.

24. McClure, J. W.: Theory of Diamagnetism of Graphite. Phys. Rev.. vol. 119, no. 2, July 15, 1960, pp. 606-613.

25. Inoue, Masaharu: Landau Levels and Cyclotron Resonance in Graphite. J. Phys. Soc. Japan, vol. 17, no. 5, May 1962, pp. 808-819.

26. Laurence, James C.: High-Field Electromagnets at NASA Lewis Research Center. NASA TN D-4910, 1968.

27. Woollam, J. A.: Evanohm Resistance to 18 T (180 kG) at 4.2 K. Rev. Sci. Instr., vol. 41, no. 2, Feb. 1970, pp. 284-285.

28. Long, J. R.; Grenier, C. G.; and Reynolds, J. M.: Electron and Lattice Transport Phenomena in an Antimony Crystal at Liquid-He^4 Temperatures. Phys. Rev., vol. 140, no. 1A, Oct. 4, 1965, pp. 187-201.

29. Woollam, J. A.: Spin Splitting, Fermi Energy Changes, and Anomalous g Shifts in Single Crystal and Pyrolytic Graphite. Phys. Rev. Letters 25 (1970).

NASA-Langley, 1970 — 26 E-5696

"The aeronautical and space activities of the United States shall be conducted so as to contribute . . . to the expansion of human knowledge of phenomena in the atmosphere and space. The Administration shall provide for the widest practicable and appropriate dissemination of information concerning its activities and the results thereof."

—NATIONAL AERONAUTICS AND SPACE ACT OF 1958

NASA SCIENTIFIC AND TECHNICAL PUBLICATIONS

TECHNICAL REPORTS: Scientific and technical information considered important, complete, and a lasting contribution to existing knowledge.

TECHNICAL NOTES: Information less broad in scope but nevertheless of importance as a contribution to existing knowledge.

TECHNICAL MEMORANDUMS: Information receiving limited distribution because of preliminary data, security classification, or other reasons.

CONTRACTOR REPORTS: Scientific and technical information generated under a NASA contract or grant and considered an important contribution to existing knowledge.

TECHNICAL TRANSLATIONS: Information published in a foreign language considered to merit NASA distribution in English.

SPECIAL PUBLICATIONS: Information derived from or of value to NASA activities. Publications include conference proceedings, monographs, data compilations, handbooks, sourcebooks, and special bibliographies.

TECHNOLOGY UTILIZATION PUBLICATIONS: Information on technology used by NASA that may be of particular interest in commercial and other non-aerospace applications. Publications include Tech Briefs, Technology Utilization Reports and Technology Surveys.

Details on the availability of these publications may be obtained from:

SCIENTIFIC AND TECHNICAL INFORMATION OFFICE

NATIONAL AERONAUTICS AND SPACE ADMINISTRATION

Washington, D.C. 20546